Incorporating Power System Stability Metrics into the Optimal Power Flow

Ashutossh Gupta, Manish K. Singh, and Vassilis Kekatos

***Abstract*— While the effect of network topology, line impedances, and (synthetic) inertia/damping coefficients of synchronous generators and distributed energy resources (DER) on dynamic performance have been extensively investigated, the impact of the power network operating point has not been studied. This work proposes a novel semi-definite program (SDP)-based optimal power flow (OPF) formulation to find a more stable generator dispatch. Different stability metrics widely used in industry can be captured by a carefully selected $\mathcal{H}_2$-norm of a linear time-invariant (LTI) system obtained from swing dynamics. Under practical approximations, the dependence of this norm on the operating point can be captured by a convex model. This allows selecting the operating point to minimize stability metrics, generation costs, or combinations thereof through an SDP-based OPF. A two-stage approach can also be followed, where first, active power setpoints are decided by a standard OPF, and reactive power setpoints are decided subsequently by the proposed OPF. Pareto optimality analysis carried out to study the relative trade-off between generation and stability costs reveals that a significant improvement in stability can be obtained with small increments in generation cost. Dynamic simulations on the IEEE 68-bus system corroborate that the found OPF schedules feature improved dynamic behavior.**

I. Introduction

Power systems constantly experience disturbances of varying magnitudes and time scales, which can lead to sustained oscillations or even power outages. This fact renders system stability a sought-after attribute. Along with rotor angle, voltage magnitude, and frequency stability, resonance, and converter-driven stability also need to be considered due to the addition of HVDC, FACTs, and power-electronic converter-based devices [1], [2]. Most studies aim to design control mechanisms to enhance system stability. However, stability also relies on the initial operating conditions a system is subject to. In transmission networks, rotor angle stability has been studied based on the effect of large and small disturbances, called transient and small-signal stability, respectively. While transient stability has been incorporated in finding stable operating points [3], studies optimizing over small-signal stability metrics to obtain generator dispatches are relatively sparse.

Small-signal stability studies have focused on ensuring that the state transition matrix of linearized power system dynamics have negative real parts. Several works aim at either perturbing or obtaining operating points while minimizing the spectral abscissa [4]. Such methods require computing eigenvalues iteratively and are challenged by the non-smoothness of spectral abscissa [4]. With the evolving understanding of stability [1], studies have aimed to classify system stability using various metrics based on the intended application. Popular industry metrics include event-based measures of frequency nadir, settling times, frequency deviations from the center of inertia, network coherence, short circuit current during faults [5], [6], and have been incorporated into unit commitment [7] and resource planning studies [8]. System theoretic metrics invoked in analytical studies include the $\mathcal{H}_2$ and $\mathcal{H}_\infty$ norms of appropriately defined linear dynamical systems [9], [10], [11]. Planning studies optimize the previous metrics while selecting network topologies and line impedances, placing virtual inertia and damping through inverter-interfaced resources, and designing controllers [9], [12]. However, investigations on the effect of the operating point of such stability metrics are relatively sparse. While the planning studies involving sophisticated metrics assume a fixed operating point, most works pursuing stability-improving operating points are challenged by the computationally burdensome notion of spectral abscissa [13]. Although [14] obtains a stability-promoting OPF by minimizing the $\mathcal{H}_2$-norm of linearized system dynamics, it uses gradient updates that might miss the global optimum.

In this work, we capture various industry-relevant stability metrics using the $\mathcal{H}_2$-norm of an LTI system and connect them to the operating point of a power system using a novel SDP-based formulation of the OPF. This formulation can utilize additional reactive power support provided by DERs to enhance system stability. Although the proposed formulation relies on a constant damping assumption, numerical tests demonstrate the approach's effectiveness even when the assumption is waived. Along with studying the Pareto front between generation cost and stability metric, we also suggest and numerically evaluate a *two-stage* approach, similar to the one suggested in [15]. This two-stage approach decides active power setpoints based on the standard OPF formulation and, subsequently, decides reactive power setpoints on an OPF that minimizes the stability cost. The obtained operating points are validated by simulating system responses due to load variations in a practical system with heterogeneous damping and third-order machine models.

The rest of the paper is organized as follows. Section II reviews the algebraic and dynamic power system model. Section III includes different stability metrics, their connection to the $\mathcal{H}_2$-norm of an LTI system, and a convex reformulation of the $\mathcal{H}_2$-norm. The stability-aware SDP-

This work was partially supported by the U.S. NSF under grant 1923221.

Ashutossh Gupta and Vassilis Kekatos are with the Elmore Family School of Electrical and Computer Engineering, Purdue University, West Lafayette, Indiana USA (emails: {gupta799,kekatos}@purdue.edu).

Manish K. Singh is with the Department of Electrical and Computer Engineering, University of Wisconsin–Madison, Madison, Wisconsin, USA (email: manish.singh@wisc.edu)

based OPF is presented in Section IV and numerically validated in Section V. Section VI concludes the article.

II. System Modeling

A power transmission system can be represented by a graph $\mathcal{G} = (\mathcal{N}, \mathcal{L})$. The set of nodes $\mathcal{N}$ includes the $N+1$ buses indexed by $n \in \mathcal{N} := \{0, 1, \ldots, N\}$, and the set of edges $\mathcal{L}$ the transmission lines indexed by $\ell = (m, n) \in \mathcal{L}$, where $m, n \in \mathcal{N}$. Set $\mathcal{N}$ constitutes a collection of generation, load, and zero-injection buses. Load buses may represent sub-transmission networks with DERs connected to them. If needed, buses hosting DERs can provide reactive power support to enhance grid dynamic stability. For reasons to be discussed later, we collectively refer to load and generation buses as *synchronous buses* contained in set $\mathcal{S} \subset \mathcal{N}$ indexed by $n = 0, \ldots, S$. Zero-injection buses are collected in set $\bar{\mathcal{S}} = \mathcal{N} \setminus \mathcal{S}$, and indexed by $n = S+1, \ldots, N$.

Let vector $\mathbf{v}$ collect the complex voltages $v_n = V_n \angle \theta_n$ for all buses $n \in \mathcal{N}$. Each synchronous bus $n \in \mathcal{S}$ can be modeled as an internal voltage source $e_n = E_n \angle \delta_n$ connected to the terminal bus via reactance $x_n > 0$. The current flowing from the internal to the terminal bus n is $\frac{e_n - v_n}{jx_n}$. While $\mathbf{v}$ governs OPF studies, vector $\mathbf{e}$ collecting all internal voltages governs swing power system dynamics. Ignoring shunts, the two voltage vectors are related through Ohm's law as [16]:

$$\begin{bmatrix} \mathbf{Y}_{\mathcal{S},\mathcal{S}} & \mathbf{Y}_{\mathcal{S},\bar{\mathcal{S}}} \\ \mathbf{Y}_{\mathcal{S},\bar{\mathcal{S}}}^\top & \mathbf{Y}_{\bar{\mathcal{S}},\bar{\mathcal{S}}} \end{bmatrix} \begin{bmatrix} \mathbf{v}_{\mathcal{S}} \\ \mathbf{v}_{\bar{\mathcal{S}}} \end{bmatrix} = \begin{bmatrix} \mathbf{Y}_{\mathcal{S}}(\mathbf{e} - \mathbf{v}_{\mathcal{S}}) \\ \mathbf{0} \end{bmatrix} \tag{1}$$

where the left-hand side involves the bus admittance matrix partitioned into synchronous and non-synchronous buses, and the diagonal matrix $\mathbf{Y}_{\mathcal{S}} = \mathrm{dg}(\{1/(jx_n)\})$ collects all internal reactances. Eliminating buses in $\bar{\mathcal{S}}$ provides:

$$\mathbf{v}_{\mathcal{S}} = \mathbf{\Gamma} \mathbf{Y}_{\mathcal{S}} \mathbf{e}. \tag{2}$$

where matrix $\mathbf{\Gamma} := (\mathbf{Y}_{\mathcal{S},\mathcal{S}} + \mathbf{Y}_{\mathcal{S}} - \mathbf{Y}_{\mathcal{S},\bar{\mathcal{S}}} \mathbf{Y}_{\bar{\mathcal{S}},\bar{\mathcal{S}}}^{-1} \mathbf{Y}_{\mathcal{S},\bar{\mathcal{S}}}^\top)^{-1}$ is known to exist [17]. Equation (2) relates terminal to internal voltages and, thus, couples OPF to dynamic stability studies. We next review models for the OPF and swing dynamics.

Optimal power flow (OPF) models are expressed in terms of $\mathbf{v}$ and typically involve the ensuing constraints:

$$\mathbf{v}^H \mathbf{M}_{p_n} \mathbf{v} = p_n^g - \bar{p}_n^d \qquad \forall n \in \mathcal{S} \tag{3a}$$

$$\mathbf{v}^H \mathbf{M}_{q_n} \mathbf{v} = q_n^g - q_n^d \qquad \forall n \in \mathcal{S} \tag{3b}$$

$$\underline{p}_n^g \le p_n^g \le \bar{p}_n^g \qquad \forall n \in \mathcal{S} \tag{3c}$$

$$\underline{q}_n^g \le q_n^g \le \bar{q}_n^g \qquad \forall n \in \mathcal{S} \tag{3d}$$

$$(1 - \alpha_n)\bar{q}_n^d \le q_n^d \le (1 + \alpha_n)\bar{q}_n^d \qquad \forall n \in \mathcal{S} \tag{3e}$$

$$\underline{v}_n \le \mathbf{v}^H \mathbf{M}_{v_n} \mathbf{v} \le \bar{v}_n \qquad \forall n \in \mathcal{N} \tag{3f}$$

$$\mathbf{v}^H \mathbf{M}_{i_{mn}} \mathbf{v} \le \bar{i}_{mn} \qquad \forall (m, n) \in \mathcal{L} \tag{3g}$$

Constraints (3a)–(3b) relate net complex power injections to terminal voltages using appropriately defined $(N+1) \times (N+1)$ Hermitian matrices $(\mathbf{M}_{p_n}, \mathbf{M}_{q_n})$ [18]. Constraints (3c)–(3d) impose limits on power generation. Symbol $\bar{p}_n^d$ denotes the fixed active load demand at bus n. Constraint (3e) allows reactive power demands to vary by $\pm\alpha_n$ off their nominal values $\bar{q}_n^d$. Selecting $\alpha_n = 0$ for all buses yields standard OPF formulations. Positive α_n's expand the OPF feasible set and capture the capability for additional reactive power support by DERs to improve on generation costs, grid stability, and/or other operational objectives [14]. Constraint (3f) confines squared voltage magnitudes V_n^2 within given ranges with $\mathbf{M}_{v_n} = \mathbf{e}_n \mathbf{e}_n^\top$, where $\mathbf{e}_n$ is the n-th canonical vector. Constraint (3g) limits squared current magnitudes per line ratings. If y_{mn} is the series impedance of line $(m, n) \in \mathcal{L}$, the current flowing on this line is $i_{mn} = (v_m - v_n) y_{mn}$, so that $\mathbf{M}_{i_{mn}} = |y_{mn}|^2 (\mathbf{e}_m - \mathbf{e}_n)(\mathbf{e}_m - \mathbf{e}_n)^\top$.

We proceed with *dynamic stability models* [19]. The active power injection p_n is the active power flow over reactance x_n across internal voltage e_n and terminal voltage v_n:

$$p_n = \frac{E_n V_n}{x_n} \sin(\delta_n - \theta_n) = \frac{1}{x_n} \mathrm{Im}\{e_n v_n^*\}. \tag{4}$$

Eliminating v_n from (4) using (2) provides [19]:

$$p_n = \sum_{k=0}^{S} \frac{E_n E_k}{x_n x_k} \mathrm{Re}\left\{ \Gamma_{nk} \cdot e^{j(\delta_n - \delta_k)} \right\}.$$

Because $|\mathrm{Re}\{\Gamma_{nk}\}| \ll |\mathrm{Im}\{\Gamma_{nk}\}|$ under a lossless power system model, the previous expression simplifies as

$$p_n = \sum_{k=0}^{S} \frac{E_n E_k}{\gamma_{nk}} \sin(\delta_n - \delta_k). \tag{5}$$

where $\gamma_{nk} := -(x_n x_k)/\mathrm{Im}(\Gamma_{nk}) > 0$ serves as the *effective reactance* between the synchronous machines connected to buses k and n, and is symmetric $\gamma_{nk} = \gamma_{kn}$ [16].

Let the synchronous machine connected to bus $n \in \mathcal{S}$ be associated with frequency $\omega_n = \dot{\delta}_n$ and inertia/damping constants M_n and D_n. Recall that the complex phasor representation $E_n \angle \delta_n(t)$ corresponds to a sinusoidal voltage waveform $\sqrt{2} E_n \cos(\omega t + \delta_n(t))$, where ω is the nominal angular frequency. Frequency ω_n represents the deviation from the nominal and should be close to zero. Swing dynamics for the synchronous machine n dictate [2]

$$M_n \dot{\omega}_n + D_n \omega_n = p_n^g - p_n - \bar{p}_n^d \tag{6}$$

where p_n^g, p_n, and p_n^d denote respectively the mechanical power input, the electric power flowing from bus n to the grid, and the power demand at bus n. While (6) applies to bus n, injection p_n couples all $S+1$ machines via (5).

Collect $\{\omega_n\}_{n \in \mathcal{S}}$ and $\{\delta_n\}_{n \in \mathcal{S}}$ in $\boldsymbol{\omega}$ and $\boldsymbol{\delta}$. Let the state tuple $(\boldsymbol{\omega}^0, \boldsymbol{\delta}^0)$ correspond to an equilibrium of (6) so that $\dot{\omega}_n = 0$ for all n. We are interested in frequency-synchronized solutions of (6) implying that $\boldsymbol{\omega}^0 = \omega^0 \mathbf{1}$. Because $\sum_{n=0}^{S} p_n = 0$ from (5), one obtains

$$\omega^0 = \frac{\sum_{n=0}^{S} p_n^{\mathrm{in}}}{\sum_{n=0}^{S} D_n}$$

where $p_n^{\mathrm{in}} := p_n^g - p_n^d$ is the net power entering the system at bus n.

Assume for convenience that $\sum_{n=0}^{S} p_n^{\mathrm{in}} = 0$ and so $\omega^0 = 0$ at steady state. This is without loss of generality: If the assumption is violated, one can seamlessly resort to a change

of variables $\tilde{\omega}_n(t) = \omega_n(t) - \omega^0$, $\tilde{p}_n^{\text{in}}(t) = p_n^{\text{in}}(t) - \omega^0 D_n$, and $\tilde{\delta}_n(t) = \delta_n(t) - \omega^0 t$. Proceeding with $\omega^0 = 0$, we note from (5)–(6) that the angles $\boldsymbol{\delta}^0$ at equilibrium are such that

$$p_n^{\text{in}} = p_n = \sum_{k=0}^{S} \frac{E_n E_k}{\gamma_{nk}} \sin(\delta_n^0 - \delta_k^0). \tag{7}$$

We next obtain a linear time-invariant (LTI) system by linearizing (6) at the equilibrium point. To this end, we assume constant voltage magnitudes and consider small perturbations in (p_n^{in}, p_n) to $(p_n^{\text{in}} + \Delta p_n^{\text{in}}, p_n + \Delta p_n)$ corresponding to angles $\delta_n^0 + \Delta\delta_n$. Linearizing (5) provides

$$\Delta \mathbf{p} \simeq \mathbf{L}_{\boldsymbol{\delta}^0} \Delta \boldsymbol{\delta} \tag{8}$$

where $\Delta\mathbf{p}$ collects $\{\Delta p_n\}_{n=0}^S$, vector $\Delta\boldsymbol{\delta}$ collects $\{\Delta\delta_n\}_{n=0}^S$, and the Jacobian matrix $\mathbf{L}_{\boldsymbol{\delta}^0}$ is evaluated at $\boldsymbol{\delta} = \boldsymbol{\delta}^0$ with entries

$$[\mathbf{L}_{\boldsymbol{\delta}^0}]_{nk} = \begin{cases} \sum_{m \neq n} \frac{E_n E_m}{\gamma_{nm}} \cos(\delta_n^0 - \delta_m^0) & , \ n = k \\ -\frac{E_n E_k}{\gamma_{nk}} \cos(\delta_n^0 - \delta_k^0) & , \ n \neq k. \end{cases} \tag{9}$$

Note that $\gamma_{nk} > 0$ and $|\delta_n^0 - \delta_k^0| < \pi/2$ holds for admissible power system operating points. The Jacobian is a graph Laplacian matrix and is known to be positive semidefinite [20].

Let diagonal matrices $\mathbf{M}$ and $\mathbf{D}$ carry the inertia and damping coefficients per unit, respectively. Linearizing (6) for all buses in $\mathcal{S}$ and substituting (8) yields

$$\mathbf{M}\dot{\boldsymbol{\omega}} + \mathbf{D}\boldsymbol{\omega} + \mathbf{p} + \mathbf{L}_{\boldsymbol{\delta}^0}\Delta\boldsymbol{\delta} = \mathbf{p}^{\text{in}} + \Delta\mathbf{p}^{\text{in}}. \tag{10}$$

The steady-state operating schedules of input powers $\mathbf{p}$ and injected powers $\mathbf{p}^{\text{in}}$ cancel out due to (7). Note that $\boldsymbol{\omega} = \dot{\boldsymbol{\delta}}^0 + \Delta\dot{\boldsymbol{\delta}} = \Delta\dot{\boldsymbol{\delta}}$, and hence, vector $\boldsymbol{\omega}$ actually represents the deviation of bus frequencies from nominal. Therefore, all states and inputs of the LTI system in (10) involve deviations from their nominal values. For notational brevity, we will henceforth omit the Δ's. The linearized dynamics of (10) can be endowed with the state-space model [20]:

$$\begin{bmatrix} \dot{\boldsymbol{\delta}} \\ \dot{\boldsymbol{\omega}} \end{bmatrix} = \underbrace{\begin{bmatrix} \mathbf{0} & \mathbf{I} \\ -\mathbf{M}^{-1}\mathbf{L}_{\boldsymbol{\delta}^0} & -\mathbf{M}^{-1}\mathbf{D} \end{bmatrix}}_{\mathbf{A}:=} \begin{bmatrix} \boldsymbol{\delta} \\ \boldsymbol{\omega} \end{bmatrix} + \underbrace{\begin{bmatrix} \mathbf{0} \\ \mathbf{M}^{-1} \end{bmatrix}}_{\mathbf{B}:=} \mathbf{p}^{\text{in}} \tag{11a}$$

$$\mathbf{y} = \underbrace{\begin{bmatrix} \mathbf{C}_{11} & \mathbf{0} \\ \mathbf{0} & \mathbf{C}_{22} \end{bmatrix}}_{\mathbf{C}:=} \begin{bmatrix} \boldsymbol{\delta} \\ \boldsymbol{\omega} \end{bmatrix} \tag{11b}$$

where the vector of observables $\mathbf{y}$ collects K_δ outputs related to voltage angles and K_ω outputs related to voltage frequencies. Because observables associated with angles and frequencies are typically disparate, it is customary to impose a block-diagonal structure on matrix $\mathbf{C}$ with $\mathbf{C}_{11} \in \mathbb{R}^{K_\delta \times (S+1)}$ and $\mathbf{C}_{22} \in \mathbb{R}^{K_\omega \times (S+1)}$. Critically, the presented dynamics relate to the operating point of the power system through the Jacobian $\mathbf{L}_{\boldsymbol{\delta}^0}$ appearing in $\mathbf{A}$. The LTI system of (11) will be referred to as system H. We next review how commonly used grid stability metrics relate to $\mathbf{y}$ for proper choices of $\mathbf{C}$.

III. Stability Metrics and Operating Point

One common metric of system stability is *network coherence*. It quantifies how much voltage angles differ from their network average. It can be expressed as $\|\mathbf{y}(t)\|_2^2$ by selecting $\mathbf{C}_{11} = \mathbf{I} - \frac{1}{S+1}\mathbf{1}\mathbf{1}^\top$ and $\mathbf{C}_{22} = \mathbf{0}$ in (11b); see [10]. In large multi-area systems, area-wise coherency may be more practical. Such metric can be captured by $\|\mathbf{y}(t)\|_2^2$ upon choosing a block-diagonal $\mathbf{C}_{11}$. To capture oscillations on the power flow across line $(m,n) \in \mathcal{L}$, the operator may use the stability metric $(\delta_m(t) - \delta_n(t))^2$ corresponding to $\mathbf{C}_{11} = (\mathbf{e}_m - \mathbf{e}_n)^\top$. We reserve $f_\delta(t)$ to denote any stability metric related only to voltage angles ($\mathbf{C}_{22} = \mathbf{0}$).

Stability metrics of interest can also be imposed on voltage angular frequencies. One such metric is *synchrony* [5], defined as the sum of squared frequency deviations from the *center of inertia* $\bar{\omega}(t) := \frac{\sum_{n=0}^S M_n \omega_n(t)}{\sum_{n=0}^S M_n}$. Synchrony can be expressed as $\|\mathbf{y}(t)\|_2^2$ by setting $\mathbf{C}_{11} = \mathbf{0}$ and $\mathbf{C}_{22} = \mathbf{I} - \frac{1}{\mathbf{1}^\top\mathbf{M}\mathbf{1}}\mathbf{1}\mathbf{1}^\top\mathbf{M}$. A simpler stability metric is the sum of squared frequency excursions obtained by setting $\mathbf{C}_{22} = \mathbf{I}$. Metrics on angular frequencies alone ($\mathbf{C}_{11} = \mathbf{0}$) will be denoted by $f_\omega(t)$.

Different stability metrics can be captured by the output norm $\|\mathbf{y}(t)\|_2^2$ of the system H for appropriate choices of $\mathbf{C}$. However, the output norm varies with time and depends on input $\mathbf{p}^{\text{in}}(t)$. We are interested in a cost function capturing stability that is time-independent. The $\mathcal{H}_2$-norm is a commonly used measure for quantifying the stability of LTI systems [21]. Given the LTI system H in (11), its $\mathcal{H}_2$-norm can be computed as $\|H\|_{\mathcal{H}_2}^2 = \text{Tr}(\mathbf{B}^\top\mathbf{Q}\mathbf{B})$. Matrix $\mathbf{Q}$ is the observability Grammian and can be found as the solution to the Lyapunov equation $\mathbf{A}^\top\mathbf{Q} + \mathbf{Q}\mathbf{A} = -\mathbf{C}^\top\mathbf{C}$.

The $\mathcal{H}_2$-norm is defined only for stable systems. Because $\mathbf{L}_{\boldsymbol{\delta}^0}$ is a Laplacian, matrix $\mathbf{A}$ in (11) has $[\mathbf{1}^\top \ \mathbf{0}^\top]^\top$ in its nullspace. All other system poles are strictly in the negative complex half-plane, hence resulting in a marginally stable system. The marginally stable eigenvector of $\mathbf{A}$ corresponds to a common shift in $\boldsymbol{\delta}$. Because voltage angles are defined with respect to a reference anyway, a uniform shift is often non-detectable, and Assumption 1 hold in practice [10].

Assumption 1. *The outputs are chosen such that* $\mathbf{C}_{11}\mathbf{1} = \mathbf{0}$.

Thanks to Assumption 1, system H is BIBO stable and its $\mathcal{H}_2$-norm is finite [9]. The way norm $\|H\|_{\mathcal{H}_2}^2$ relates to $\|\mathbf{y}(t)\|_2^2$ is amenable to various interpretations [10]:

i1) The expected steady-state value of an angle-based stability metric for unit-variance white noise input $\mathbf{p}^{\text{in}}(t)$:

$$\|H\|_{\mathcal{H}_2}^2 = \lim_{t\to\infty} \mathbb{E}\left[\|\mathbf{y}(t)\|_2^2\right] = \lim_{t\to\infty} \mathbb{E}\left[f_\delta(t)\right];$$

i2) The sum of time-integrals of an angle-based stability metric $f_\delta^n(t)$ for unit-impulse disturbances $\mathbf{p}_n^{\text{in}}(t) = \mathbf{e}_n\delta(t)$[1]:

$$\|H\|_{\mathcal{H}_2}^2 = \sum_{n=0}^{S} \int_0^\infty f_\delta^n(t)\,\mathrm{d}t.$$

[1]Note that $\delta(t)$ denotes the Dirac delta (impulse) function, whereas $\delta_n(t)$ denotes the voltage angle of machine n. Moreover, vector $\mathbf{e}_n$ denotes the n-th canonical vector, whereas e_n is the internal voltage at bus $n \in \mathcal{S}$.

i3) The sum of time-integrals of a frequency-based stability metric $f_\omega^n(t)$ for unit-step disturbances $\mathbf{p}_n^{\text{in}}(t) = \mathbf{e}_n u(t)$:

$$\|H\|_{\mathcal{H}_2}^2 = \sum_{n=0}^{S} \int_0^\infty f_\omega^n(t)\, \mathrm{d}t.$$

Matrix $\mathbf{A}$ depends on the operating point via $\mathbf{L}_{\boldsymbol{\delta}^0}$. In turn, norm $\|H\|_{\mathcal{H}_2}^2$ depends on $\mathbf{A}$ through $\mathbf{Q}$ being the solution of the Lyapunov equation. Aiming for a more stable system operation, one may attempt to find an OPF dispatch yielding smaller $\|H\|_{\mathcal{H}_2}^2$. Norm $\|H\|_{\mathcal{H}_2}^2$ has been optimized before over inertia coefficients or transmission topologies [9], [12].

Unfortunately, norm $\|H\|_{\mathcal{H}_2}^2$ is not amenable to a convenient expression over $\mathbf{v}$ or the generation setpoints [9], [5]. Nonetheless, under Assumption 1, this $\mathcal{H}_2$-norm can be bounded as [9]:

$$\|H_c(D_{\max})\|_{\mathcal{H}_2}^2 \leq \|H\|_{\mathcal{H}_2}^2 \leq \|H_c(D_{\min})\|_{\mathcal{H}_2}^2 \tag{12}$$

where $D_{\min} := \min_{n\in\mathcal{S}} D_n$ and $D_{\max} := \max_{n\in\mathcal{S}} D_n$ are the minimum and maximum damping coefficients, and

$$\|H_c(D)\|_{\mathcal{H}_2}^2 := \frac{1}{2D}\left(\mathrm{Tr}(\mathbf{C}_{11}^\top \mathbf{C}_{11} \mathbf{L}_{\boldsymbol{\delta}^0}^\dagger) + \mathrm{Tr}(\mathbf{C}_{22}^\top \mathbf{C}_{22} \mathbf{M}^{-1})\right)$$

is the $\mathcal{H}_2$-norm of an LTI system $H_c(D)$ obtained upon simplifying the original system H by setting $\mathbf{D} = D\mathbf{I}_S$ in (11). In other words, system $H_c(D)$ has constant damping across all buses. Matrix $\mathbf{L}_{\boldsymbol{\delta}^0}^\dagger$ is the pseudo-inverse of $\mathbf{L}_{\boldsymbol{\delta}^0}$.

Rather than minimizing $\|H\|_{\mathcal{H}_2}^2$, we aim at minimizing $\|H_c(D)\|_{\mathcal{H}_2}^2$ for some D and leverage its favorable analytic expression. The bounds in (12) become tighter when damping coefficients lie in a limited range. The latter typically holds when damping coefficients are expressed in per unit.

Clearly, if the stability criterion of interest relates solely to frequencies ($\mathbf{C}_{11} = \mathbf{0}$), norm $\|H_c(D)\|_{\mathcal{H}_2}^2$ becomes independent of $\mathbf{L}_{\boldsymbol{\delta}^0}$ and depends only on the inertia and damping parameters. Nonetheless, in such cases the operating point still affects frequency dynamics. Specifically, basic linear system theory dictates that the *step response* of voltage frequencies coincides with the *impulse response* of voltage angles; contrast interpretations *i2)* and *i3)* earlier. Therefore, if one is interested in studying a stability metric $f_\omega(t)$ obtained by choosing $(\mathbf{C}_{11}, \mathbf{C}_{22}) = (\mathbf{0}, \mathbf{C}_\omega)$ under a step disturbance, it suffices to choose $(\mathbf{C}_{11}, \mathbf{C}_{22}) = (\mathbf{C}_\omega, \mathbf{0})$ and analyze the resulting impulse response of $\|\mathbf{y}(t)\|_2^2$. Such reformulation enables us to study the effect of the operating point and network parameters on the frequency dynamics of the power network as well. We next incorporate $\|H_c(D)\|_{\mathcal{H}_2}^2$ into OPF models.

IV. Stability-Cognizant Optimal Power Flow

To balance between economic efficiency and grid stability, we put forth the ensuing stability-cognizant OPF model:

$$\begin{aligned} \min \quad & (1-\lambda)\sum_{n\in\mathcal{S}} c_n^p p_n^g + \lambda \|H_c(D)\|_{\mathcal{H}_2}^2 \\ \text{over} \quad & \mathbf{v}, \mathbf{e}, \mathbf{L}_{\boldsymbol{\delta}^0}, \{p_n^g, q_n^g, q_n^d\}_{n\in\mathcal{S}} \\ \text{s.to} \quad & (2), (3), (9). \end{aligned} \tag{13}$$

The model trades generation cost for grid stability, with the latter captured by the approximate norm $\|H_c(D)\|_{\mathcal{H}_2}^2$. The precise value of D is apparently inconsequential as it appears as a constant scaling factor in $\|H_c(D)\|_{\mathcal{H}_2}^2$. By solving (13) for different values of $\lambda \in [0,1]$, a system operator can obtain the Pareto front across the two objectives.

Albeit constraint (2) is linear in $(\mathbf{v}, \mathbf{e})$, standard OPF constraints in (3) and the definition of $\mathbf{L}_{\boldsymbol{\delta}^0}$ in (9) are non-convex: OPF constraints are quadratic in $\mathbf{v}$ and matrix $\mathbf{L}_{\boldsymbol{\delta}^0}$ is quadratic in $\mathbf{e}$. *Variable lifting* is a known trick to bypass the non-convexity of (3): Introduce a matrix variable $\mathbf{V} = \mathbf{v}\mathbf{v}^H$, express standard OPF constraints linearly in $\mathbf{V}$, eliminate variable $\mathbf{v}$, and enforce $\mathbf{V}$ to be positive semidefinite and rank-1. Because rank constraints are non-convex, drop the rank-1 constraint to relax the OPF into a semidefinite program (SDP) [18]. If the minimizer $\mathbf{V}^*$ turns out to be rank-1, the SDP relaxation of the OPF is deemed *exact*.

Interestingly, variable lifting can also alleviate the non-convexity of $\mathbf{L}_{\boldsymbol{\delta}^0}$ in terms of $\mathbf{e}$. Constraint (9) can be expressed as a linear constraint on the *lifted* matrix variable $\mathbf{E} := \mathbf{e}\mathbf{e}^H$ as

$$[\mathbf{L}_{\boldsymbol{\delta}^0}]_{nk} = \begin{cases} \sum_{m\neq n} \frac{\mathrm{Re}\{E_{nm}\}}{\gamma_{nm}} & ,\ n = k \\ -\frac{\mathrm{Re}\{E_{nk}\}}{\gamma_{nk}} & ,\ n \neq k. \end{cases} \tag{14}$$

Variable $\mathbf{e}$ can be eliminated as long as the relation between $(\mathbf{v}, \mathbf{e})$ from (2) is passed onto $(\mathbf{V}, \mathbf{E})$. This is possible by imposing constraint (15e). In [19], we adopted variable lifting to minimize inter-area oscillations. Here, we aim at a broad class of stability metrics captured as the $\mathcal{H}_2$-norm of an LTI system that can be posed as SDPs.

Minimizing $\|H_c(D)\|_{\mathcal{H}_2}^2$ over $\mathbf{L}_{\delta^0}$ entails minimizing $\mathrm{Tr}(\mathbf{C}_{11}^\top \mathbf{C}_{11} \mathbf{L}_{\boldsymbol{\delta}^0}^\dagger)$. The latter can be further simplified according to the ensuing result, whose proof is a simple generalization of [22, Lemma 1] and is omitted.

Lemma 1. *For $\mathbf{W} := \mathbf{C}_{11}^\top \mathbf{C}_{11}$, let $\tilde{\mathbf{W}}$ and $\tilde{\mathbf{L}}_{\boldsymbol{\delta}^0}$ be the $S \times S$ matrices obtained after removing the first row and first column from $\mathbf{W}$ and $\mathbf{L}_{\boldsymbol{\delta}^0}$, respectively. If Assumption 1 holds, then*

$$\mathrm{Tr}(\mathbf{W}\mathbf{L}_{\boldsymbol{\delta}^0}^\dagger) = \mathrm{Tr}(\tilde{\mathbf{W}}\tilde{\mathbf{L}}_{\boldsymbol{\delta}^0}^{-1}).$$

Using variable lifting and Lemma 1, the OPF in (13) can be reformulated as the following SDP:

$$\begin{aligned} \min \quad & (1-\lambda)\sum_{n\in\mathcal{S}} c_n^p p_n^g + \lambda\,\mathrm{Tr}(\mathbf{X}) && (\text{OPF}_\lambda) \\ \text{over} \quad & \mathbf{X}, \mathbf{V}, \mathbf{E}, \tilde{\mathbf{L}}_{\boldsymbol{\delta}^0}, \{p_n^g, q_n^g, q_n^d\}_{n\in\mathcal{S}} \\ \text{s.to} \quad & (3c)-(3e),\ (14) \\ & \mathrm{Tr}(\mathbf{M}_{p_n}\mathbf{V}) = p_n^g - \bar{p}_n^d && \forall n \in \mathcal{S} \quad (15a) \\ & \mathrm{Tr}(\mathbf{M}_{q_n}\mathbf{V}) = q_n^g - q_n^d && \forall n \in \mathcal{S} \quad (15b) \\ & \underline{v}_n \leq \mathrm{Tr}(\mathbf{M}_{v_n}\mathbf{V}) \leq \bar{v}_n && \forall n \in \mathcal{N} \quad (15c) \\ & \mathrm{Tr}(\mathbf{M}_{i_{mn}}\mathbf{V}) \leq \bar{i}_{mn} && \forall (m,n) \in \mathcal{L} \quad (15d) \\ & \mathbf{V}_{\mathcal{S},\mathcal{S}} = \boldsymbol{\Gamma}\mathbf{Y}_{\mathcal{S}}\mathbf{E}\mathbf{Y}_{\mathcal{S}}^H\boldsymbol{\Gamma}^H && (15e) \\ & \begin{bmatrix} \mathbf{X} & \tilde{\mathbf{W}}^{1/2} \\ \tilde{\mathbf{W}}^{1/2} & \tilde{\mathbf{L}}_{\boldsymbol{\delta}^0} \end{bmatrix} \succeq 0 && (15f) \end{aligned}$$

$$\mathbf{V} \succeq 0, \mathbf{E} \succeq 0 \tag{15g}$$

where $\mathbf{V}_{\mathcal{S},\mathcal{S}}$ is the submatrix obtained upon selecting only the first $(S+1)$ rows and columns of $\mathbf{V}$. By Schur's complement, constraint (15f) is equivalent to $\tilde{\mathbf{L}}_{\boldsymbol{\delta}^0} \succ 0$ and $\mathbf{X} \succeq \tilde{\mathbf{W}}^{1/2}\tilde{\mathbf{L}}_{\boldsymbol{\delta}^0}^{-1}\tilde{\mathbf{W}}^{1/2}$. The former holds by the definition of $\mathbf{L}_{\boldsymbol{\delta}^0}$ in (14). The latter holds with equality if $\lambda > 0$, in which case $\mathrm{Tr}(\mathbf{X}) = \mathrm{Tr}(\tilde{\mathbf{W}}\tilde{\mathbf{L}}_{\boldsymbol{\delta}^0}^{-1})$ at optimality. The relaxed stability-cognizant OPF is deemed *exact* if the optimal $\mathbf{V}$, and consequently $\mathbf{E}$, are rank-1.

Two-stage OPF model: Problem (OPF$_\lambda$) can be useful to a system operator in different ways. For $\lambda = 0$, we get the plain (OPF$_0$), for which constraints (15e)–(15g) and $\mathbf{E} \succeq 0$ should be dropped. For $\lambda = 1$, problem (OPF$_1$) aims at minimizing the approximate stability metric alone. Because (OPF$_1$) may yield higher generation costs, the operator may decide to first solve (OPF$_0$) and decide $\{p_n^g\}_{n\in\mathcal{S}}$. The operator may subsequently solve (OPF$_1$) to decide $\{q_n^g\}_{n\in\mathcal{S}}$ and/or $\{q_n^d\}_{n\in\mathcal{S}}$ while $\{p_n^g\}_{n\in\mathcal{S}}$ are set to the values decided by (OPF$_0$). We denote this two-stage model as (OPF$_{0\to1}$).

V. Numerical Tests

The proposed OPF models were numerically tested on the IEEE 68-bus system using YALMIP with solver Mosek. The network parameters, generator limits, nominal loads, inertia, and damping coefficients were obtained from Power Simulation Toolbox (PST) data files [23]. We emulated DERs on load buses having virtual inertia 10^{-2} p.u. and damping coefficients drawn randomly from a normal distribution with mean 10^{-2} and standard deviation 10^{-3}. Upon eliminating zero-injection buses, the benchmark system was reduced to 51 buses. We used identical costs $c_n^p = 1$ across all generators. To ensure exactness of (OPF$_\lambda$), a small resistance of 10^{-4} pu was added to all lossless network branches. Network coherence and line flow oscillation across transmission line 1-2 were selected as the stability metrics. Line 1-2 is a major inter-tie, prone to low-frequency inter-area oscillations.

To study the exactness of the SDP relaxation, we evaluated the ratio of the largest to the second largest eigenvalue of OPF solution $\mathbf{V}$ recovered by (OPF$_\lambda$) using the two stability metrics. This ratio was more than $1,000$ for all $\lambda \in [0,1]$ and for both $\alpha_n = 0$ and $\alpha_n = 0.3$. Thus, problem (OPF$_\lambda$) gives nearly rank-1 solutions of $\mathbf{V}$, indicating the relaxation to be exact for different problem instances.

To explore the trade-off between generation and stability costs, (OPF$_\lambda$) was solved for different $\lambda \in [0,1]$ and at full load. Figure 1 shows the obtained Pareto fronts with network coherence as the stability metric. Recall that (OPF$_\lambda$) minimizes $\|H_c(D_{\min})\|_{\mathcal{H}_2}^2$, which is an upper bound of the actual stability cost $\|H\|_{\mathcal{H}_2}^2$. Interestingly, the Pareto front reveals that the relative improvement in $\|H_c(D_{\min})\|_{\mathcal{H}_2}^2$ roughly coincides with the relative improvement in $\|H\|_{\mathcal{H}_2}^2 = \mathrm{Tr}(\mathbf{B}^\top\mathbf{Q}\mathbf{B})$. The Pareto front without reactive power support by DERs ($\alpha_n = 0$) shows that the stability metric can be improved by 8.48% at the expense of raising generation costs by 0.33%. If not aiming for the most stable operation, a significant improvement in stability can be attained with

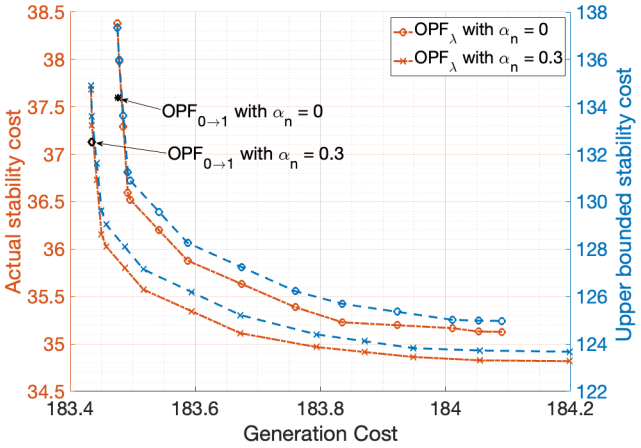

Fig. 1. Pareto front obtained by single-stage (OPF$_\lambda$) for $\lambda \in [0,1]$ under network coherence as stability metric, with ($\alpha_n = 0.3$) and without ($\alpha_n = 0$) reactive power support by DERs. Improvements in stability metric achieved by two-stage (OPF$_{0\to1}$) are also shown For each operating point, the left y-axis shows the actual stability metric $\|H\|_{\mathcal{H}_2}^2$, while the right y-axis shows the approximated stability metric $\|H_c(D)\|_{\mathcal{H}_2}^2$.

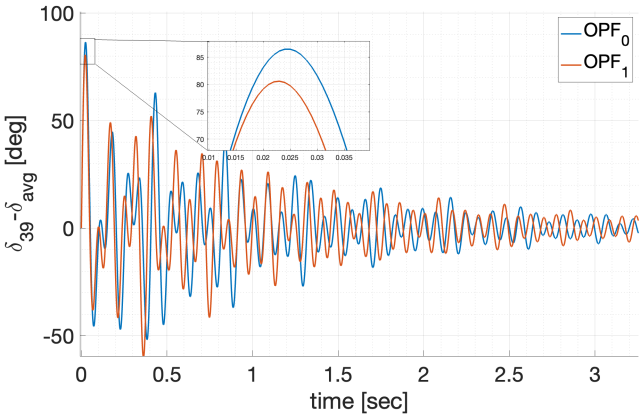

Fig. 2. Deviations of voltage angle at bus 39 from average due to a 1-pu impulse change at load bus 39.

a marginal increase in generation cost. For instance, the stability metric can be reduced by 7.92% for only a 0.17% increase in generation cost. Further, the two-stage (OPF$_{0\to1}$) model improved stability by 2.85% at the same generation cost as (OPF$_0$). Similar observations can be inferred from the Pareto front obtained with $\alpha_n = 0.3$.

Similarly, evaluating (OPF$_0$) and (OPF$_1$) with line flow oscillation as the stability metric, we observed an improvement of 13.14% in $\|H\|_{\mathcal{H}_2}^2$ (around 11.93% with $\alpha = 0.3$), while the increase in generation cost was only by around 0.5% in both cases. The two-stage OPF reduced the stability cost by 5.28% for $\alpha_n = 0$, and 3.50% for $\alpha_n = 0.3$. These results show the flexibility of (OPF$_\lambda$) in finding more stable operating points. Moreover, it utilizes reactive power support by DERs to improve stability for a lesser increase in generation cost.

We also evaluated system dynamics due to load variations at different operating points obtained from (OPF$_\lambda$). Although (OPF$_\lambda$) considers only swing dynamics, our tests included

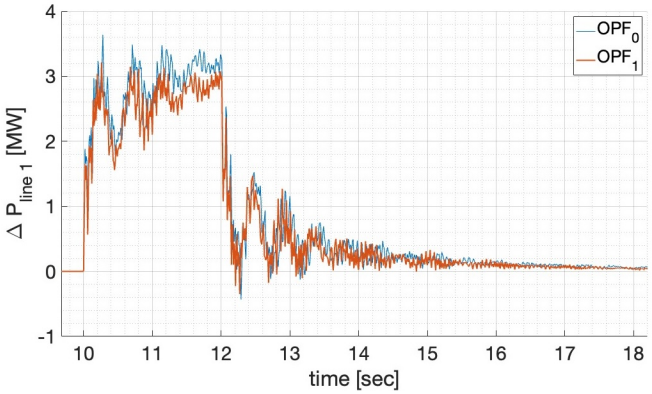

Fig. 3. Flow deviations on line 1-2 due to a 0.1-pu pulse change at bus 2.

third-order machine models with droop coefficients $r_n = 0.04$ p.u. and turbine time constant $\tau_n = 0.4$ sec. For DERs, this resembles the commonly used droop-control-based strategy for inverter operation. Comparing the network coherence obtained under (OPF_0) and (OPF_1) setpoints, the maximum value reduces from 1.55 to 1.45, an improvement of about 7%. This corresponds to a maximum of 6° reduction in voltage angle excursions from their average across buses. For instance, Figure 2 depicts the angle deviations from the average at load bus 39. Note that summed-up bus frequency deviations from the COI frequency under a step disturbance would also follow a similar trend; refer to discussion in Sec. III. Figure 3 shows the deviations in active power flow along line 1-2 caused by 0.1-pu load change at bus 2 that lasted for 2 seconds. Thanks to (OPF_1) with the line flow stability metric, the maximum line flow excursions are reduced by 15%. The settling time was also reduced. These results indicate the effectiveness of (OPF_λ) towards improving dynamics at a system or component (critical intertie) level.

VI. Conclusions

Commonly used stability metrics and their dependence on the operating point have been approximately captured through a convex model. Thanks to this model, operating points of enhanced stability can be identified through an SDP-OPF. Numerical tests demonstrate that the SDP relaxation enjoys a practically rank-one solution under different stability metrics, generation costs, and combinations thereof. Stability metrics can be reduced significantly at the expense of minimal increases in generation costs. Such increases become smaller when DERs provide additional reactive power support as the feasible space of the OPF widens. Stability metrics can be global (network coherence) or local (line flow oscillations). Dynamic simulations on a practical system corroborate that the found schedules feature lower nadir, faster settling times, and/or reduced flow oscillations.

References

[1] N. Hatziargyriou, J. V. Milanovic, and et.al., "Definition and classification of power system stability- revisited & extended," *IEEE Trans. Power Syst.*, vol. 36, no. 4, pp. 3271–3281, Jul. 2021.

[2] P. Kundur, *Power system stability and control*. New York, NY: McGraw-Hill, 1994.

[3] T. Chen, A. Y. Lam, Y. Song, and D. J. Hill, "Fast tuning of transmission power flow routers for transient stability constrained optimal power flow under renewable uncertainties," *Electric Power Systems Research*, vol. 213, p. 108735, 2022.

[4] P. Li, J. Qi, J. Wang, H. Wei, X. Bai, and F. Qiu, "An SQP method combined with gradient sampling for small-signal stability constrained OPF," *IEEE Trans. Power Syst.*, vol. 32, no. 3, pp. 2372–2381, May 2017.

[5] F. Paganini and E. Mallada, "Global analysis of synchronization performance for power systems: bridging the theory-practice gap," *IEEE Trans. Automat. Contr.*, vol. 65, no. 7, pp. 3007–3022, Jul 2020.

[6] S. S. Guggilam, C. Zhao, E. Dall'Anese, Y. C. Chen, and S. V. Dhople, "Optimizing DER participation in inertial and primary-frequency response," *IEEE Trans. Power Syst.*, vol. 33, no. 5, pp. 5194–5205, 2018.

[7] Z. Chu and F. Teng, "Stability constrained optimization in high IBR-penetrated power systems-Part II: Constraint validation and applications," 2024. [Online]. Available: https://arxiv.org/abs/2307.12156

[8] ——, "Coordinated planning for stability enhancement in high ibr-penetrated systems," 2024. [Online]. Available: https://arxiv.org/abs/2404.14012

[9] B. K. Poolla, S. Bolognani, and F. Dorfler, "Optimal placement of virtual inertia in power grids," *IEEE Trans. Automat. Contr.*, vol. 62, no. 12, pp. 6209–6220, Dec. 2017.

[10] E. Tegling, B. Bamieh, and D. Gayme, "The price of synchrony: Evaluating the resistive losses in synchronizing power networks," *IEEE Trans. Control of Network Systems*, vol. 2, no. 3, pp. 254–66, Sep. 2015.

[11] V. Häberle, M. W. Fisher, E. Prieto-Araujo, and F. Dörfler, "Control design of dynamic virtual power plants: An adaptive divide-and-conquer approach," *IEEE Trans. Power Syst.*, vol. 37, no. 5, pp. 4040–4053, Nov. 2021.

[12] S. Bhela, H. Nagarajan, D. Deka, and V. Kekatos, "Efficient topology design algorithms for power grid stability," *IEEE Control Systems Lett.*, vol. 6, pp. 1100–1105, Jun. 2021.

[13] P. Pareek and H. D. Nguyen, "A convexification approach for small-signal stability constrained optimal power flow," *IEEE Trans. Control of Network Systems*, vol. 8, no. 4, pp. 1930–1941, 2021.

[14] M. Inoue, T. Sadamoto, M. Arahata, and A. Chakrabortty, "Optimal power flow design for enhancing dynamic performance: Potentials of reactive power," *IEEE Trans. Smart Grid*, vol. 12, no. 1, pp. 599–611, 2020.

[15] J. Wang, Y. Song, D. J. Hill, Y. Hou, and F. Fan, "Stability constrained OPF in microgrids: A chance constrained optimization framework with non-Gaussian uncertainty," 2023. [Online]. Available: https://arxiv.org/abs/2302.02168

[16] T. Ishizaki, A. Chakrabortty, and J.-I. Imura, "Graph-theoretic analysis of power systems," *Proc. IEEE*, vol. 106, no. 5, pp. 931–952, May 2018.

[17] F. Dorfler and F. Bullo, "Kron reduction of graphs with applications to electrical networks," *IEEE Trans. Circuits Syst. I*, vol. 60, no. 1, pp. 150–163, Jan. 2013.

[18] S. H. Low, "Convex relaxation of optimal power flow—Part I: Formulations and equivalence," *IEEE Trans. Control of Network Systems*, vol. 1, no. 1, pp. 15–27, 2014.

[19] M. K. Singh and V. Kekatos, "Optimal power flow schedules with reduced low-frequency oscillations," in *in Proc. Power Systems Computation Conference*, Porto, Portugal, Jun. 2021.

[20] B. Gentile, J. Simpson-Porco, F. Dorfler, S. Zampieri, and F. Bullo, "On reactive power flow and voltage stability in microgrids," in *Proc. IEEE American Control Conf.*, Portland, OR, Jun. 2014, pp. 759–764.

[21] I. Khalil, J. Doyle, and K. Glover, *Robust and optimal control*. Englewood Cliffs, NJ: Prentice Hall, 1996, vol. 2.

[22] S. Bhela, D. Deka, H. Nagarajan, and V. Kekatos, "Designing power grid topologies for minimizing network disturbances: An exact MILP formulation," in *Proc. IEEE American Control Conf.*, Philadelphia, PA, 2019, pp. 1949–1956.

[23] J. H. Chow and K. W. Cheung, "A toolbox for power system dynamics and control engineering education and research," *IEEE Trans. Power Syst.*, vol. 7, no. 4, pp. 1559–1564, Nov. 1992.